ARKIV FÖR FYSIK Band 19 nr 38

Communicated 8 March 1961 by The Svedberg and Erik Rudberg

Total nuclear reaction cross sections for 180 MeV protons

By A. Johansson, U. Svanberg and O. Sundberg

With 4 figures in the text

ABSTRACT

The total nuclear reaction cross sections for 180 MeV protons incident on Li, Be, C, Al, Ca, Fe, In and Au have been measured. Range separation was used to distinguish between elastically and inelastically scattered particles and the effect of the shape of the range curve was studied. The total rms errors are 2–3 % and mainly due to counting statistics.

The experimental cross sections have been compared with the results of a calculation using an optical model with parameters derived from the Gammel-Thaler nucleon-nucleon scattering matrix.

1. Introduction

The optical model which has been commonly used to analyse experimental data on the elastic scattering of protons from nuclei is also capable of predicting the total reaction cross section. In this connection a "reaction" means an interaction in which the proton leaves the nucleus in an excited state or transforms it into another nucleus; i.e. all nuclear interactions are included except elastic scattering. The measurements reported in this paper were made at a bombarding energy of 180 MeV with the main purpose of reducing the ambiguity in the optical model analysis of elastic scattering at that energy. In particular, one would expect the imaginary part only of the potential to determine the reaction cross section quite well, whereas all terms contribute to the differential cross sections and polarizations. The details of the analysis are reported in the following paper [1].

Total reaction cross sections for nucleons incident on nuclei have been studied previously and the experiments concerned with protons as bombarding particles at energies between 30 and 900 MeV are listed in Table 1 together with some relevant experimental parameters. In all cases the attenuation in intensity of a proton beam by an attenuator (target) was measured, but the experiments may be divided into two groups according to the different methods of detecting protons emerging from the target. In the 134, 860 and 895 MeV experiments a detector that was insensitive to the proton energy was used and the reaction cross sections were obtained by extrapolation to zero solid angle of the poor geometry loss cross sections. Certain assumptions regarding the angular distributions of elastically and inelastically scattered particles had to be satisfied, which made the extrapolation procedure somewhat uncertain and the method not very easy to use when aiming at accuracies of the

Table 1. Measurements of the total reaction cross section for protons at bombarding energies between 30 and 900 MeV.

Mean proton energy (MeV)	Energy band width (MeV)	Level below which inelastic events are excluded (MeV)	Elements studied	Ref.
34	5	0	C, Al, Fe, Sn, Pb	Gooding [2]
61	5	0	C, Al, Fe, Sn, Pb	Meyer *et al.* [3]
77	10	0	C, Al, Cu, Ag, Pb	Goloskie, Strauch [4]
95	10	0	C, Al, Cu, Ag, Pb	Goloskie, Strauch [4]
113	10	0	C, Al, Cu, Ag, Pb	Goloskie, Strauch [4]
133	10	0	C, Al, Cu, Ag, Pb	Goloskie, Strauch [4]
134	26	0	C, Al, Cu, Cd, Pb	Cassels, Lawson [5]
180	10	0	Li, Be, C, Al, Ca, Fe, In, Au	This experiment
185	45	20	Be, C, Al, Cu, Pb, U	Kirschbaum [6]
240	65	20	Be, C, Al, Cu, Pb, U	Kirschbaum [6]
305	65	20	Be, C, Al, Cu, Pb, U	Kirschbaum [6]
230	220	15	U	Millburn *et al.* [7]
290	100	15	C, Al, Cu, U	Millburn *et al.* [7]
860	60	0	Be, C, Al, Cu, Sn, Pb	Chen *et al.* [8]
895	70	0	C, Al, Cu, Sb, Pb	Booth *et al.* [9]

order of a few percent. In principle, however, the separation of elastic and inelastic events was complete. The use of an energy-sensitive detector for the emerging particles—as in all other experiments listed—introduced a means to set a separation level for inelastic events, i.e. to discriminate against protons having lost a certain amount of energy in the target in excess of the ionization loss. Thus the reaction cross sections could be obtained more directly. The separation level is indicated in the table, 0 MeV meaning that the inelastic contribution has been corrected for. As the protons lose energy in the target by ionization the value obtained for the cross section is an average value over an often considerable energy range. This may not be too serious, however, as the energy dependence of the cross sections seems to be slight. Table 1 shows that when the present experiment was started there existed an early determination of the reaction cross section for a few nuclei at about the same bombarding energy. As that determination was of a rather exploratory nature a remeasurement with improved accuracy was considered to be well motivated.

2. Description of the experiment

2.1. *General considerations*

As in all attenuation experiments the equipment was designed to measure the number N_0 of nearly monoenergetic protons incident on an attenuator (= target) and the number N_1 of protons that emerge from the target without having caused any reaction. The total reaction cross section, σ, can then be obtained from

$$N_1/N_0 = \exp(-n\sigma) \tag{1}$$

or

$$\frac{N_0 - N_1}{N_0} = n\sigma \quad \text{for} \quad n\sigma \ll 1,$$

where n denotes the number of nuclei per cm² in the target. As the detectors used were 100 % efficient for proton detection, N_0 and N_1 were not statistically independent—every proton contributing to N_1 must have been included in N_0—and there was nothing to be gained by trying to obtain the difference N_0–N_1 by anticoincidence methods. The standard deviation in the ratio N_1/N_0 is given by the binomial distribution formula

$$\Delta\left(\frac{N_1}{N_0}\right)=\frac{1}{\sqrt{N_0}}\cdot\sqrt{\frac{N_1}{N_0}\left(1-\frac{N_1}{N_0}\right)}. \tag{2}$$

The elastically scattered protons were distinguished from those inelastically scattered and from other reaction products by range separation. An absorber was inserted between the target and the detector for emerging particles. The energy resolution was then necessarily limited by the combined effects of multiple Coulomb scattering and range straggling in this absorber. Target thicknesses and the geometrical properties of the proton beam were chosen in such a way that their combined effect on energy resolution should be small. Naturally some elastically scattered protons caused reactions in the absorber; i.e. the number actually counted was not N_1 but $N_2=\eta\cdot N_1$, where η is the chance for an elastic proton to penetrate the absorber. The coefficient η was determined experimentally in a "target-out" measurement, where the incident beam energy was reduced by an amount corresponding to the target thickness. This gave

$$\eta=N_2'/N_0', \tag{3}$$

where the prime denotes target-out measurements. Equation (1) then becomes

$$\frac{N_2}{N_0}\cdot\frac{N_0'}{N_2'}=\exp\left(-n\,\sigma\right). \tag{4}$$

The target thicknesses were chosen so that the protons lost 9 MeV by ionization. This corresponded to $n\sigma$ approximately equal to 0.02 and as η was about 0.79 a statistical accuracy of 1 % in the cross section would require a total number of incident protons of 1.4×10^7. This could be reached in about 30 hours effective counting time, the limitation being the electronically allowable counting rate.

2.2. *The proton beam*

The experimental lay-out is shown in Fig. 1. As the requirements on the proton beam properties were very stringent the ordinary external beam from the cyclotron had to be modified. Four collimators were used at different positions along the proton path, marked A, B, C and D in Fig. 1. The collimator at B was a 10 mm thick brass piece with a circular aperture of 3 mm diameter. Its main purpose was to reduce the geometrical cross section of the beam. The thickness was not sufficient to stop protons from going through the wall, but on the other hand edge scattering was kept small. At A the outer part of the proton beam was clipped, where the protons still had one turn left inside the cyclotron. The reason for the clipping was that it eliminated one of the two beams which would otherwise have appeared at C. The collimators C and D were sufficiently large to let the main beam, i.e. protons coming through the aperture at B, pass without touching the edges. When the beam arrived at C it also contained

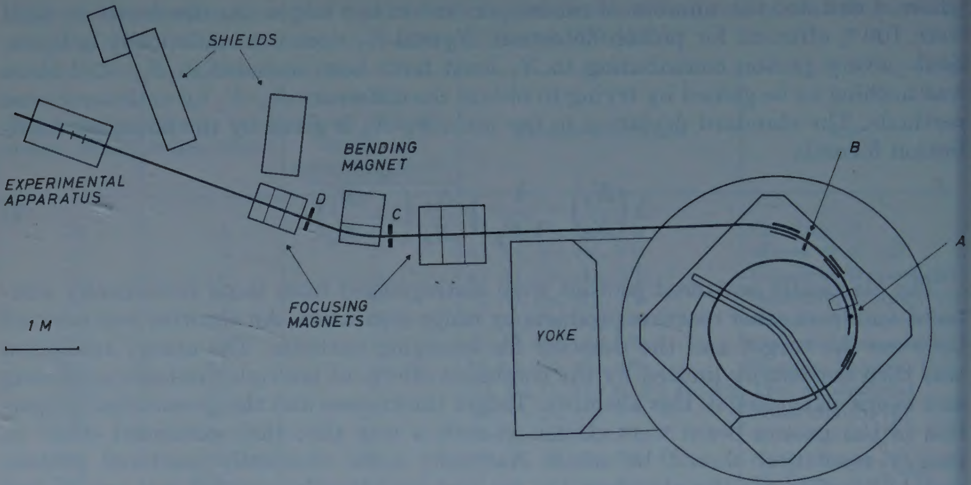

Fig. 1. The general lay-out of the experiment.

a smooth background of low-energy particles. The small percentage of this tail that could pass through the aperture at C was made to miss the opening at D by the use of a bending magnet. Photographic methods were used to determine collimator sizes, and, in particular, heavy overexposures of photographic paper at D and at the exit of the last focusing magnet indicated that the beam was free from low-energy ionizing particles. Neutrons which were produced at C and D by the low-energy tail were negligible due to the very small solid angle of the counter when seen from D. Also the neutrons produced at A and B and in the magnetic channels inside the cyclotron were negligible due to the large distance from the detecting apparatus and the shields used.

The beam was focused on the target by two pairs of quadrupole magnets, both of which were necessary to handle the large astigmatism of the beam emerging from the cyclotron. At optimum focusing the beam cross section at the entrance of the apparatus was approximately circular with a diameter of 0.7 mm. The maximum angular spread obtained from the picture taken at the exit of the last focusing magnet, where the beam was also almost circular and had a diameter of 6–7 mm, was $\pm 0.09°$. This was completely negligible in comparison with the rms angular spread due to multiple Coulomb scattering in the Mylar foil, in the pre-absorber and in the first two counters which added up to about 0.4°. The size of the beam at the target was, however, essentially unaffected by this spread because the counters were very close to the target.

The beam was always carefully aligned to pass through the centre of the detecting apparatus. The photographic methods used allowed a determination of the beam position to at least ± 0.2 mm at the scatterer and of its angular deviation from the symmetry axis to $\pm 0.04°$.

During the runs the beam intensity had to be reduced in order not to overload the electronic circuits. In fact, the ion source of the cyclotron was turned off completely.

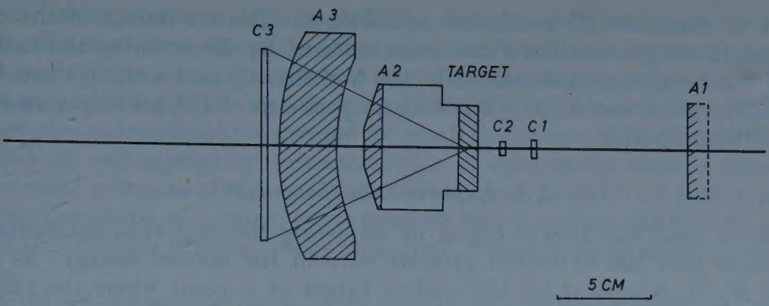

Fig. 2. The detector arrangement.

2.3. *Apparatus*

The detector arrangements are shown in Fig. 2. The letters A and C refer to absorbers of various materials and to scintillators (counters) respectively. The beam left the vacuum tube through a thin Mylar foil as close as possible to the first absorber. $C1$ and $C2$ in coincidence gave directly the number of incident protons N_0. Their dimensions were $10 \times 10 \times 3$ mm³ and $7 \times 7 \times 3$ mm³ respectively. The 4 mm thick counter $C3$ was circular with a diameter of 100 mm and its distance from the target so chosen that it covered scattering angles up to 25°. The number N_2 was obtained as the number of coincidences between $C2$ and $C3$. The absorbers $A2$ and $A3$ were shaped to give the same separation level between elastic and inelastic scattering events for all scattering angles; i.e. at a separation level of ΔE MeV the absorber thickness, experienced by a particle which had been scattered at an arbitrary angle ($< 25°$) and lost ΔE MeV to the target nucleus in excess of the recoil energy loss, was equal to its mean range. This condition could only be exactly satisfied for one point in the target which was, of course, taken to be the middle but because of the small dimension of the beam and the relatively thin targets it was approximately true for all possible places of scattering.

The aluminium absorber $A2$ was 10 MeV thick in the forward direction and shaped to compensate for recoil energy loss whereas the main part of the energy reduction occurred in the copper absorber $A3$, which consequently was of the correct shape for an infinitely heavy target nucleus and a plane parallel $A2$. As the recoil losses are different for different nuclei, each target had to have a separate absorber $A2$; they were, in fact, mounted in pairs on a wheel with remote control for placing an arbitrary target in the beam. The absorber $A1$ was variable in eight steps and made it possible to measure at various points on the range curve. It was made of polythene in order to minimize small angle scattering from it.

The light pulses from the scintillators (NE102) were guided onto RCA6810 A photomultipliers from which the pulses were fed into transistorized coincidence units and fast prescalers. The dead time of the circuits was sufficiently small ($= 25$ nsec) for two protons from consecutive r.f. bursts of the cyclotron to be resolved. The counting rate, however, had to be kept below about 200 protons/sec because of the finite chance of two protons to occur within the same r.f. burst, and consequently give a false ratio N_2/N_0. The dependence of this ratio on counting rates of this order was tested but no effect was observed. The resolving times of the coincidence units were 9 and 15 nsec for $C1 + C2$ and $C2 + C3$ respectively, which was found quite sufficient to eliminate all accidental coincidences. The constancy of the efficiency of $C3$ over the large scintillator area was checked by determining the ratio N_2/N_0 when $C3$ was being displaced vertically and horizontally and with all three absorbers removed. The ratio was 0.999 ± 0.001 at all positions of $C3$, all displacements tried being less than 35 mm.

2.4. *Experimental procedure*

A series of runs was always begun by adjusting the cyclotron magnetic field to such a value that the extracted protons were of the correct energy. As reference the ratio N_2/N_0 was used for the carbon target at a point where the range curve was very steep. The mean energy of the protons could by this method quickly be read to about 0.01 MeV (or 1 part in 18000) in relative measure. After that the beam was centered on the target by adjustments of the bending magnet field for side variations and the cyclotron magnetic median plane for height variations. The beam position was checked by exposing photographic paper.

As described in section 2.1., the actual runs consisted of determinations of the ratio N_2/N_0 for two situations, namely "target in" and "target out". Measurements were made at eight different positions along the range curve, i.e. for eight different thicknesses of $A1$. Three positions were chosen to be well above the knee; they constituted the actual measurements of the reaction cross section for different levels of inelastic separation. The next three positions were used to determine the slope of the range curve, which had to be very well known in order to correct for shape effects above the knee. The range curve levelled off before reaching zero as $A1$ was increased. The last two positions were chosen to determine that level. In the "target-out" measurements $A1$ was always increased by a 9 MeV thick polythene piece to compensate for the energy loss in the target. The coefficient η was thus measured at the proper energy of the protons penetrating $A2$ and $A3$. As the shape of $A2$ was slightly different for different targets the determination was made for two target-out situations (the carbon and the gold cases) in order to see if the size of the proton beam affected the N_2'/N_0' ratio. No effect was found within the statistical errors.

Errors caused by drift in the apparatus were minimized by frequent changes of targets and $A1$ thicknesses. As the mean proton energy had to be known to about 0.01 MeV the time variation of the cyclotron magnetic field was not always negligible. The energy reference mentioned above was frequently used during the measurements and corrections were applied in the calculations.

3. Evaluation of the cross sections

3.1. *The shape of the range curves*

The use of equation (4) requires that the target-in and target-out measurements are made at "corresponding points" on the two range curves, i.e. at such points that the two measurements would have been equal if no reactions had occurred in the target. The shapes of the range curves are expected to vary with the target used even in the ideal case of no nuclear reactions either in the target or in the absorbers. As the slopes at measuring points even well above the knee of the curve were not negligible due to the extreme accuracy needed (about 1 part in 10^4 in the ratio N_2/N_0 for an uncertainty in the cross section of 1 %), the different shapes had to be taken into account.

Experimentally, this was done by defining corresponding points as the points for which the distances along the range axis to the 50 % level were inversely proportional to the slopes at that level. A consistent use of corresponding points for comparison of target-in and target-out measurements not only eliminated first order shape effects but also automatically corrected for small deviations of the target thicknesses from 9 MeV as well as slightly different proton energies in the various runs.

A theoretical estimate of the errors that could be expected from such a procedure was made. The shape of a range curve near its end is mainly affected by spread in energy of the incident protons, range straggling, multiple small angle scattering and geometry.

(1) The spread in energy of the incident protons was difficult to estimate, but should not be larger than 1 MeV, which is known to be the upper limit for the energy spread of the ordinary external beam, i.e. the beam without collimators at A, B and C in Fig. 1. The exact value was not very important as its contribution to the slope of the range curve was small. In the calculations a total width of 0.6 MeV at half height was used.

(2) The range straggling was assumed to follow a Gaussian distribution with a rms spread in range ΔR ($\mathrm{g\cdot cm^{-2}}$) given by the formula (see for instance [10]).

$$(\Delta R)^2 = 0.1571\,\frac{Z}{A}\int_{T_0}^{T}\left(-\frac{dT}{d\xi}\right)^{-3} dT, \tag{5}$$

where T and T_0 denote the energies in MeV of the incident and the emerging protons respectively, $(-dT/d\xi)$ is the energy loss in $\mathrm{MeV/g\cdot cm^{-2}}$ and Z and A refer to the charge and mass numbers of the material traversed. The values for $(-dT/d\xi)$ were taken from the tables of Aron [11]. The range straggling effect was dominant and corresponded to an energy spread of the incident beam of about 2.7 MeV full width at half height. The contributions to $(\Delta R)^2$ from the different materials along the proton path are simply additive and the range straggling effect was also mainly responsible for the differences between the slopes at the 50 % level when various targets were used.

(3) A large number of small-angle deflections occur along the paths of the protons and make the actual path lengths greater than the thickness of the absorber. The theory of multiple Coulomb scattering by Molière [12] was used to estimate this effect, which was almost completely determined by the thickness of the copper absorber $A3$, as small variations of the scattering angle in the target, did not appreciably alter the path length through the absorbers because of their curved surfaces. The path length distribution caused by multiple scattering alone was calculated by the method of Bichsel and Uehling [13].

(4) Several geometrical effects might contribute to the slope of the range curve. For instance, the energy difference of protons leaving the target after being scattered elastically through 25° at the beginning or at the end of the target was 0.9 MeV. Beam width, angular spread, and misalignment should also have some effect. However, all geometrical contributions were expected to be small and regarded as included in the energy spread of the incident protons.

Assuming no inelastic events to take place but including the effects of range straggling and multiple Coulomb scattering, the theoretical range curves were calculated for the C and Au targets by the method described by Bichsel and Uehling [13]. In the range straggling parameter was also included the effect of the energy spread of the proton beam. The theoretical slopes at half height were about 5 % steeper than those found experimentally, which might be due to the use of too small an energy spread in the incident beam, contributions from the geometrical factors or errors in the energy-loss tables used [11]. This fact was not considered to be serious, however, because only relative changes are important for the choice of corresponding points. Both theoretically and experimentally the slope was 2 % smaller in the Au-target case than with the C target.

To test the correctness of the method to choose corresponding points, the range axis of the theoretical Au-curve was changed in such a way that the slope at half height coincided with that of the C-curve. Some small but significant deviations were found between the C-curve and the transformed Au-curve. These deviations were used to find the "corrections due to shape variations" listed in Table 2.

3.2. *False coincidences in N_2*

It was found that the N_2/N_0 ratio levelled off at about 5×10^{-3} for increasing Al thicknesses instead of going down to zero. One explanation for this fact would be that some protons after passing through $C1$ and $C2$ undergo (p,n)-reactions, where the neutrons proceed in the forward direction and have an appreciable chance of being detected by $C3$ either by ionization in the scintillator itself or by producing protons which can penetrate to $C3$. A rough theoretical estimate indicated that this effect might be of the order observed. Possibly also some decay gammas from nuclei excited by the protons might be detected by $C3$ and thus contribute to N_2. The effect was *not* due to accidental coincidences or beam admixtures of either neutrons or protons of exceptionally high energy.

Because of the flatness of the low level it was considered reasonable to assume that the effect produced a constant background in N_2 of coincidences not resulting from direct protons. The size of the effect was determined for each target separately and for the two target-out cases. The target-out background was slightly smaller than that with a target in position but no other significant differences were found. The number N_2 to be used in equation (4) was in all cases subtracted by the proper background determined in this manner.

3.3. *Scattering corrections*

Counter $C3$ covered scattering angles up to 25° and consequently the results had to be corrected for elastic scattering at larger angles and for inelastic scattering within that angle with so small an energy loss that the range separation used provided insufficient energy resolution. The corrections for elastic scattering were easily obtained by integrating the differential cross sections published in the following paper [1]. The uncertainties are mainly due to the poor knowledge of the limiting angle.

It was considerably more difficult to estimate how many inelastically scattered protons could reach $C3$. The corrections applied were based on published inelastic differential cross sections [14] for those elements for which data are available. In the other cases corrections were found by studying the spectra obtained in an experiment designed to measure the elastic cross sections [1].

3.4. *Other sources of error*

The protons which were scattered inelastically in the forward direction in the 9 MeV thick absorber used in the target-out measurements were, of course, included to some extent in N_0'. The change in that number due to this fact was, however, very small because of the small solid angle subtended by $C2$ as seen from the absorber; e.g. a cross section of 1 barn/steradian for inelastic scattering in the forward direction from carbon would increase the total reaction cross sections by about 1 %. The effect was neglected.

The method of choosing corresponding points could be assumed to take care of the effects due to different shapes of the range curves, but it introduced another source of error. The target-in and target-out ratios used in equation (4) were obtained for slightly different energies of the protons passing through $A2$ and $A3$. An approximate evaluation of this effect was made from the known energy variation (see Fig. 3) of the reaction cross section. The results are given in Table 2.

After correction of each separate measurement of the N_2/N_0 ratios for drift in proton energy, the spread in the values was compared with the spread expected from equation (2). The agreement was excellent in all cases, which indicated that no unknown source of fluctuations in the results was present.

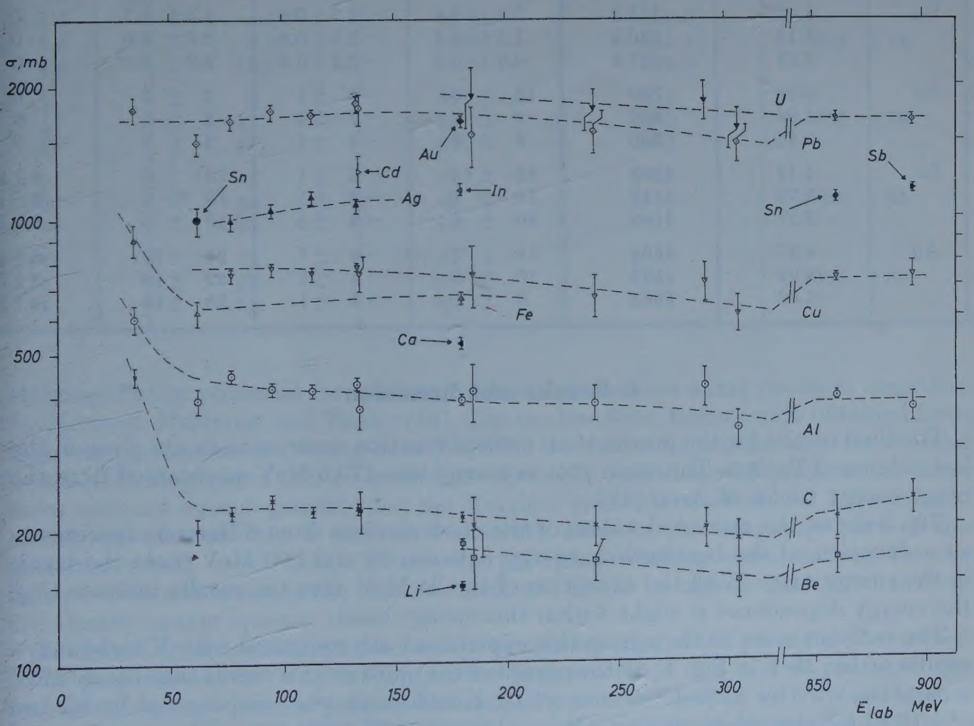

Fig. 3. The total reaction cross section for protons at bombarding energies between 30 and 900 MeV. References are given in Table 1.

Table 2. Re

All values given are in milli

Element	Level of inelastic separation (MeV)	Uncorrected cross section	Correction due to			
			inelastic scattering detected	elastic scattering at $\vartheta > 25°$	shape variations	energy di ence betw correspon points
Li	4.87	141.5	3.6 ± 1.8	−1.8 ± 0.5	0	0
	3.53	153.3	2.8 ± 1.4	−1.8 ± 0.5	0	0
	3.02	146.4	2.5 ± 1.3	−1.8 ± 0.5	0	0
Be	4.50	183.4	4.0 ± 2.0	−1.2 ± 0.3	0	0
	3.19	182.3	3.2 ± 1.6	−1.2 ± 0.3	0	0
	2.67	184.3	2.5 ± 1.2	−1.2 ± 0.3	0	0
C	4.41	204.5	1.6 ± 0.4	−1.4 ± 0.4	0	0
	3.10	216.2	0.8 ± 0.2	−1.4 ± 0.4	0	0
	2.59	215.5	0.5 ± 0.1	−1.4 ± 0.4	0	0
Al	4.48	371.1	4.6 ± 2.3	−2.6 ± 0.7	0.4 ± 0.2	0
	3.15	401.6	3.6 ± 1.8	−2.6 ± 0.7	0.8 ± 0.4	0
	2.63	387.8	2.6 ± 1.3	−2.6 ± 0.7	0.4 ± 0.2	0
Ca	4.47	511.3	3.2 ± 0.8	−2.3 ± 0.6	1.4 ± 0.7	0
	3.13	530.4	1.2 ± 0.3	−2.3 ± 0.6	2.0 ± 1.0	0
	2.61	522.9	0.9 ± 0.2	−2.3 ± 0.6	2.0 ± 1.0	0
Fe	4.29	600	12 ± 6	−2 ± 1	2 ± 1	0
	2.96	686	8 ± 4	−2 ± 1	3 ± 2	0
	2.44	660	6 ± 3	−2 ± 1	3 ± 1	0
In	4.12	1093	22 ± 11	−3 ± 1	10 ± 5	4 ± 2
	2.79	1143	14 ± 7	−3 ± 1	12 ± 6	2 ± 1
	2.27	1198	10 ± 5	−3 ± 1	10 ± 5	2 ± 1
Au	4.37	1604	14 ± 7	−4 ± 1	24 ± 12	8 ± 4
	3.04	1598	10 ± 5	−4 ± 1	32 ± 16	5 ± 3
	2.52	1668	8 ± 4	−4 ± 1	28 ± 14	4 ± 2

4. Results and discussion

The final results for the proton total nuclear reaction cross sections are given in the last column of Table 2. The mean proton energy was 179.6 MeV as obtained from the range-energy tables of Aron [11].

Fig. 3 shows the measured values of the cross sections from different experiments as a function of the bombarding energy between 30 and 900 MeV (note the break in the energy axis). With the exception of the 34 MeV data the results indicate that the energy dependence is slight within this energy band.

The reaction cross sections from this experiment are compared with Kirschbaum's results at 185 MeV in Fig. 4. As the agreement is quite good it seems that the 20 MeV separation level for inelastic events set by Kirschbaum was compensated by his use of a third counter which was sensitive only up to 20° scattering angle.

In Fig. 4 are also plotted the values for the reaction cross sections obtained in an optical model calculation. The parameters of this model were derived from the ctions and errors.

specified otherwise.

Errors (standard deviations) from			Corrected cross section	Averaged cross section and total rms errors
certainty of low-level ubtraction	uncertainty in position of corresponding points	counting statistics		
0.8	0.2	4.6	143.3	
0.8	0.9	3.7	154.3	149.0 ± 3.0
0.8	1.5	4.0	147.1	
1.3	0.3	5.6	186.2	
1.3	1.3	7.2	184.3	185.5 ± 4.5
1.3	2.3	7.4	185.6	
1.5	0.6	8.5	204.7	
1.5	2.7	6.3	215.6	212.3 ± 4.8
1.5	4.8	6.6	214.7	
3.0	1.2	17.6	373.5	
3.0	5.1	13.9	403.4	390 ± 10
3.0	8.9	14.2	388.2	
4.4	1.8	25.2	513.6	
4.4	8.0	19.9	531.3	524 ± 14
4.4	13.8	21.7	523.5	
5	3	31	612	
5	11	24	695	662 ± 19
5	21	27	667	
9	5	52	1126	
9	28	42	1168	1165 ± 34
9	43	45	1217	
14	7	81	1646	
14	28	65	1641	1660 ± 50
14	52	68	1704	

Gammel-Thaler potential for nucleon-nucleon interactions along the lines described by Kerman, McManus and Thaler [15]. The nuclear form factors were obtained from high energy electron scattering data [16]. The derivation is considered in more detail in the following paper [1]. It is evident that this optical model predicts too large cross sections except possibly for the heaviest elements studied. An approximate calculation showed that a decreased absolute value of the imaginary part of the potential would considerably reduce the predicted reaction cross sections for the lightest elements whereas the heaviest elements would be almost unaffected as they are already nearly opaque.

The effect of nuclear correlations on the imaginary part of the potential is expected to be proportional to $(V_{CR}^2 - V_{CI}^2)$ (see for instance [15]). V_{CR} and V_{CI} refer to the real and imaginary central parts of the optical potential. As V_{CR} and V_{CI} are almost equal at 180 MeV it is unlikely that the discrepancy between experimental and theoretical reaction cross sections can be explained by the neglect of nuclear correlations in the derivation of the potential parameters.

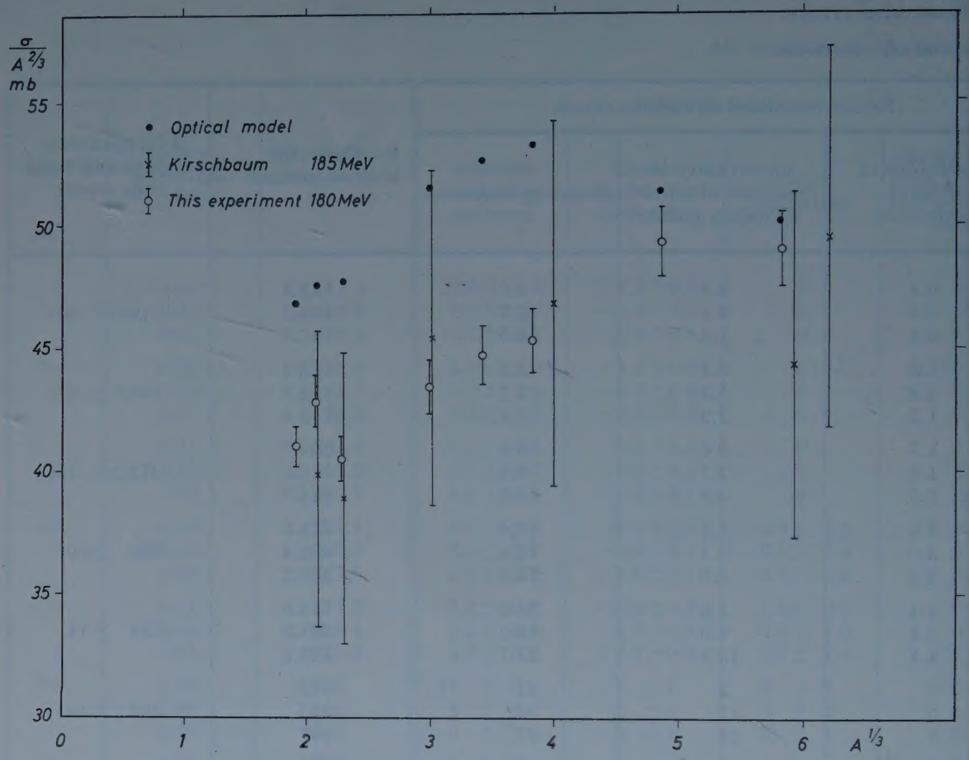

Fig. 4. The total reaction cross section for protons at 180 MeV (this experiment) and 185 MeV (Kirschbaum [6]) compared with the results of an optical model calculation. A is the mass number of the bombarded nucleus.

On the other hand it is well-known that the Gammel-Thaler scattering matrix does not fit the proton-proton scattering data extremely well at energies around 180 MeV and that the experimental information on the proton-neutron interaction is meagre. By using a more exact nucleon-nucleon scattering matrix one might therefore hope to be able to remove the discrepancy found or, conversely, the values obtained for the reaction cross sections might be useful for the study of the nucleon-nucleon interaction.

ACKNOWLEDGEMENTS

We want to thank Professor T. Svedberg for his interest in this work. The valuable help of Dr. P. E. Hodgson in performing the optical model calculations is gratefully acknowledged. As always, Mr. Å. Svanheden and the cyclotron crew were most helpful. The work was supported by the Swedish Atomic Research Council.

The Gustaf Werner Institute for Nuclear Chemistry, University of Uppsala.

REFERENCES

1. Johansson, A., Svanberg, U., and Hodgson, P. E., Arkiv Fysik *19*, 541 (1961).
2. Gooding, T. J., Nucl. Phys. *12*, 241 (1959).
3. Meyer, V., Eisberg, R. M., and Carlson, R. F., Phys. Rev. *117*, 1334 (1960).
4. Goloskie, R., and Strauch, K., Private communication.
5. Cassels, J. M., and Lawson, J. D., Proc. Phys. Soc. *67*, 125 (1954).
6. Kirschbaum, A. J., Nuclear Absorption Cross Sections for High Energy Protons, UCRL 1967 (Oct. 1952).
7. Millburn, G. P., Birnbaum, W., Crandall, W. E., and Schecter, L., Phys. Rev. *95*, 1268 (1954).
8. Chen, F. F., Lewitt, C. P., and Shapiro, A. M., Phys. Rev. *99*, 857 (1955).
9. Booth, N. E., Ledley, B., Walker, D., and White, D. H., Proc. Phys. Soc. *70*, 209 (1957).
10. Segrè, E., Exp. Nucl. Physics I, p. 244. J. Wiley & Sons, 1953.
11. Aron, W. A., The Passage of Charged Particles through Matter, UCRL 1325 (1951).
12. Molière, G., Z. Naturforsch. *3a*, 78 (1948).
13. Bichsel, H., and Uehling, E. A., Phys. Rev. *119*, 1670 (1960).
14. Tyren, H., and Maris, Th. A. J., Nucl. Phys. *4*, 637 (1957); *6*, 82, and 446 (1958); *7*, 24 (1958).
15. Kerman. A. K., McManus, H., and Thaler, R. M., Ann. Phys. *10*, 551 (1959).
16. Hofstadter, R., Ann. Rev. Nucl. Sci. *7*, 231 (1957).

Tryckt den 25 april 1961

Uppsala 1961. Almqvist & Wiksells Boktryckeri AB